AURORAL ELECTRON ENERGY ESTIMATION USING THE H/H_2 BRIGHTNESS RATIO APPLIED TO JUPITER

C. Tao*, L. Lamy†, R. Prangé†, N. André‡, and S. V. Badman§

Abstract

The measurement of the H/H_2 brightness ratio of giant planets' far-ultraviolet (FUV) aurora is a proxy for precipitating soft (a few 10s keV) electrons. We investigate the relevance of this H/H_2 indicator with the Jupiter auroral observations obtained by the Hubble Space Telescope. The H/H_2 ratio does not show any clear relationship with the FUV color ratio which is sensitive to more energetic electrons. Compared to the same analysis applied for Saturn's aurora, the relationship for Jupiter mainly shows decreasing flux with increasing energy without acceleration features.

1 Introduction

The far ultraviolet (FUV) auroral emissions of H and H_2 are commonly detected at the outer planets with H_2-dominated atmospheres. Precipitating energetic particles excite H and H_2 states, and FUV emissions are radiated when they are de-excited to the ground state.

An analysis of Saturn's southern aurora with the Ultraviolet Imaging Spectrograph (UVIS) instrument onboard the Cassini spacecraft showed that the brightness ratio of H Lyman-α to H_2 auroral emissions statistically decreases with the brightness of H_2 taken as a proxy of the energy of precipitating electrons [Lamy et al., 2013]. This ratio was suggested to provide a sensitive diagnosis of auroral electron energy from modeling studies [e.g., Rego et al., 1999], and the result observed for Saturn was investigated in detail to show that the brightness ratio provides an efficient diagnostic of low energy electrons (typically lower than 10 keV) [Tao et al., 2014; Gustin et al., 2017], in contrast with the FUV color ratio (CR), defined as the brightness ratio of a waveband unabsorbed by hydrocarbon to that

* *National Institute of Information and Communications Technology (NICT), Koganei, Japan*
† *LESIA, Observatoire de Paris–CNRS, Meudon, France*
‡ *IRAP, Université de Toulouse/UPS–OMP/CNRS, Toulouse, France*
§ *Lancaster University, Lancaster, UK*

of an absorbed one, which provides a good indicator for higher energy (> 10 keV) electrons [Gustin et al., 2009]. The energy–flux relationship of auroral electrons determined from the observations using auroral emission models shows a trend in the lower energy range (<a few keV) different to that in the higher energy range (>a few keV), reflecting different magnetosphere–ionosphere processes [Tao et al., 2014].

The auroral electron energy at Jupiter has also been estimated using FUV CR methods [e.g., Gérard et al., 2003; 2014; Gustin et al., 2016] and altitude profiles to show how deeply electrons can penetrate [e.g., Bonfond et al., 2015; Lystrup et al., 2008; Uno et al., 2014]. The typical main aurora is suggested to be produced by auroral electrons with a mean energy of several tens to hundreds of keV. In addition, precipitation of low-energy electrons (< keV to a few keV) has also been suggested to heat the Jupiter upper thermosphere [e.g., Grodent et al., 2001]. It is important to characterize this low energy electron population for understanding the entire electron energy spectrum that is injected into Jupiter's polar atmosphere. Therefore, the H/H_2 index appears relevant for Jupiter in order to investigate the role of low energy auroral electrons. In this article, we use FUV spectra taken by the Hubble Space Telescope (HST) to investigate the H/H_2 ratio of Jupiter's aurora.

2 Observation and analysis

The spectra of Jupiter were taken with the HST Space Telescope Imaging Spectrograph (STIS), using the G140L long slit configuration, during the first half of January 2014. The spectral coverage is 110−170 nm with ∼1.2 nm resolution. The spatial coverage of the slit is 52 arcsec length and 0.5 arcsec width, targeting the northern polar region parallel to the rotation axis. Time-tagged spectral observations lasting for 200 s duration were conducted for 14 orbits over two weeks. Northern polar auroral images were taken before (with a 700 s exposure) and after (with a 736 s exposure) each spectral observation. The observational details (time and geometry) are summarized in Table 1 of Tao et al. [2016a]. One image taken on January 2 is shown in Figure 1a. The spatial profile of the auroral emission at wavelengths 120−123 nm is shown in Figure 1b. The corresponding auroral regions, i.e., main aurora, high/low latitude, and Io footprint/tail, are identified visually from the image. In the following analysis, the spectral brightness of the identified region is averaged over every 30 s. Figure 2 shows summary plots of auroral images and spectra used for this analysis.

Since HST observes Jupiter from an orbit around Earth, it contains Lyman-α emissions from geo-coronal hydrogen atoms. Jupiter's coronal emission and low-latitude emission [e.g., Melin and Stallard, 2016] also contributes. We removed these contaminations by subtracting the background profile which is obtained as a hyperbolic function fitting to the intensities of the spectrum (i) just outside of limb and (ii) at a non-auroral region, as shown by the yellow line in Figure 1b. This background subtraction was applied to each 30-s averaged spectrum. This fitting of background emission is a simple assumption and a potential issue. The original observed spectra given by the black line in Figure 1c is replaced by the aurora spectrum given by the red line in the same figure after background subtraction.

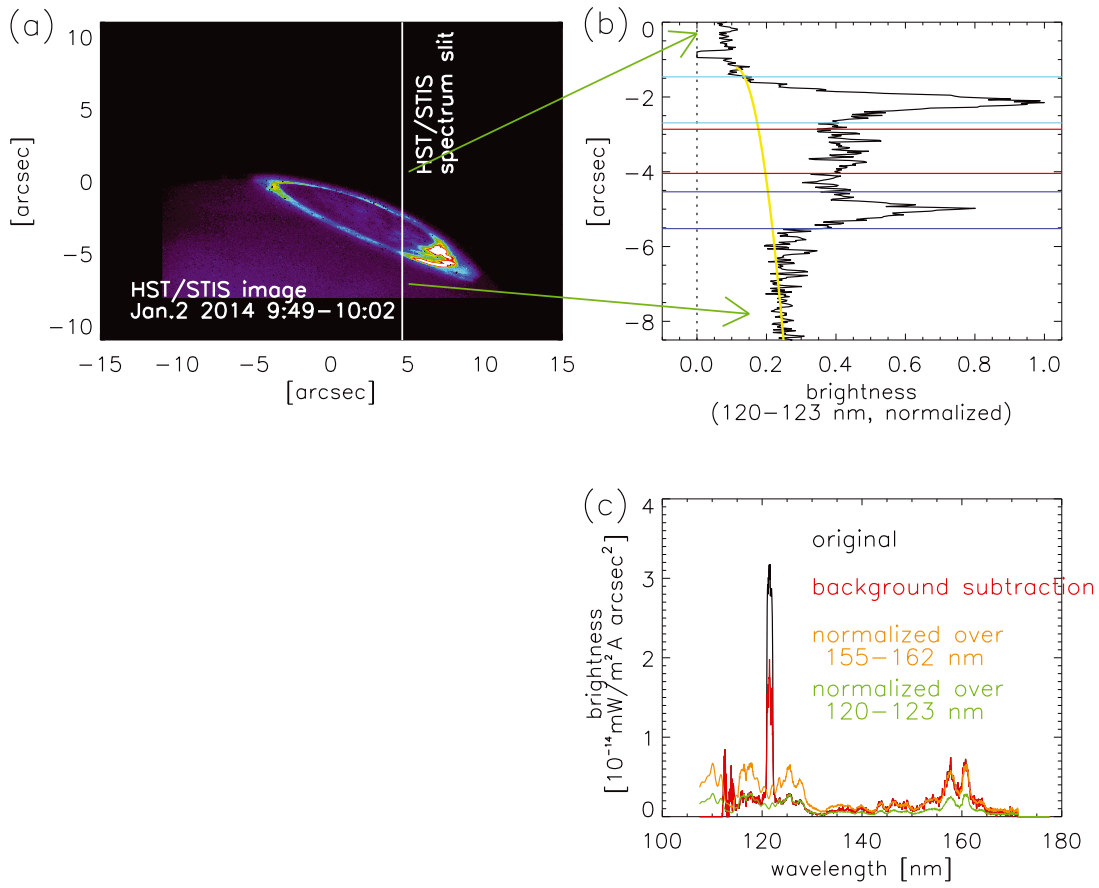

Figure 1: (a) Image of Jupiter's northern polar region, (b) spatial profile of the observed brightness integrated over wavelengths of 120–123 nm, and (c) spectral profiles, integrated over each aperture, taken on January 2, 2014. The vertical line in Figure 1a shows the position of the STIS slit for the spectral observation. The yellow curve in Figure 1b shows the background fitting (see text for detail), and horizontal lines show boundaries of the auroral regions: the main auroral emission on the disk (blue), the main auroral emission at the limb (light blue), and high latitude emission (red) seen on January 2. Lines in Figure 1c show original (black) and background–subtracted spectra (red), and fitted spectral profiles referring to spectra without (orange line) and with (green) hydrocarbon absorption.

The H/H_2 ratio is then evaluated by spectral fitting as done by Lamy et al. [2013]. We built a reference spectrum as the average of all 14 spectra. Each spectrum is integrated over the slit in the spatial direction at each aperture, and normalized by the CH_4 absorption cross-section as a function of the FUV CR, for simplicity. The FUV CR is defined as I(155–162 nm)/I(123–130 nm), where I is the height–integrated intensity of the emission in units of photons/sec over the wavelength of the subscript. Around the Lyman-α line and beyond the HST spectral range to cover 80–170 nm, we refer to the model spectrum [Tao et al., 2016b]. The reference spectrum is normalized to the intensity at 123–130 nm (green line in Figure 1c) and 144–166 nm (orange line), corresponding to the spectrum with and without hydrocarbon (HC) absorption, respectively. The green line is referred to obtain the H Lyman-α brightness above the H_2 emissions. We derive the two H/H_2 brightness ratios: H/H_2(80–170 nm) and $H/\{H+H_2$ (120–123 nm)$\}$. The H_2 total emission

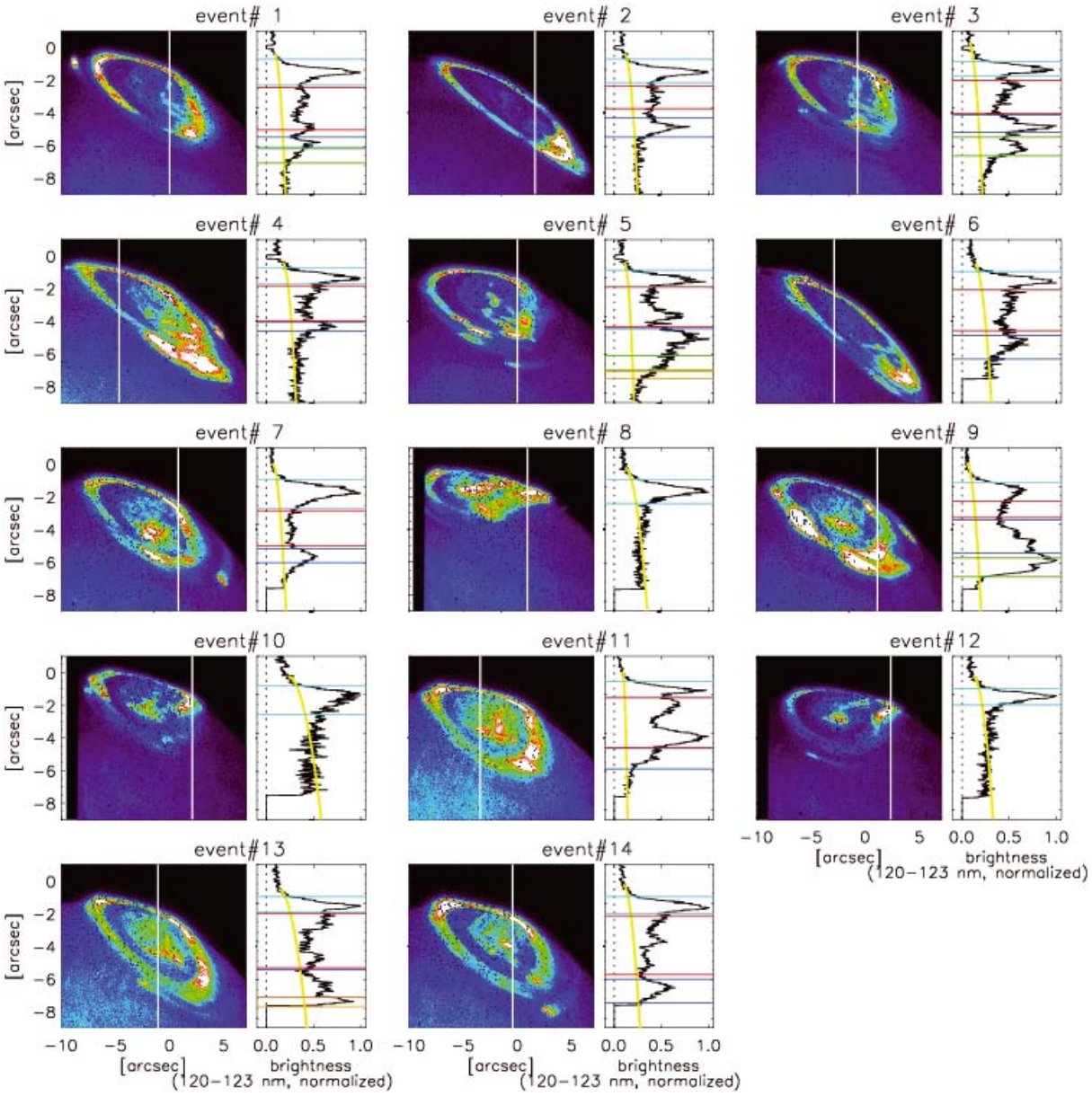

Figure 2: As Figures 1a and 1b except for image and spectra of all orbits taken on January 2014 in the program GO13035. The horizontal lines show boundaries of the auroral regions: the main aurora on the disk (blue), the main auroral emission at the limb (light blue), high latitude emission (red), low-latitude emission (green), and the Io footprint and tail (orange). The images are plotted using a linear color scale normalized for each event.

80–170 nm can be derived from the HC non-absorption waveband, 155–162 nm. Since H and H_2 (120–123 nm) experience the similar HC absorption, the latter ratio would cancel the HC absorption effect.

We convert the observed H_2 total brightness into auroral energy flux, and convert the brightness ratio H Lyman-α/H_2(80–170 nm) into electron energy considering radiative transfer of H emission, according to the conversion relation described by Tao et al. [2014], Menager et al. [2010], and references therein. Its applicability to both Saturn and Jupiter

is discussed by Tao et al. [2014]. This estimation refers to atmosphere models: the temperature profile based on Grodent et al. [2001], the neutral density profiles of main the components (H, H_2, and Helium) of Perry et al. [1999], and the hydrocarbon mixing ratios based on Gladstone et al. [1996], for the solar zenith angle of 70°. The model obtains altitudinal emission profiles considering mono-energetic electron precipitation. In addition, we simply analyze the observed integrated emission over the line of sight without considering the geometrical effect. Derived energies could be decreased by several 10s% for the FUV CR with increasing the change of viewing angles [Gustin et al., 2016]. We show the main auroral emission at the limb and on the disk separately.

3 Results

The auroral brightnesses obtained over two weeks are shown in Figure 3. The time variation of the H_2 155–162 nm band (Figure 3a, without HC absorption) and H_2 123–130 nm band (Figure 3b, with HC absorption) are similar, while that of H Lyman-α (Figure 3c) sometimes shows similar intensity variation (in DOY 10–12) but is more often different from the H_2 emissions.The relationship between the H_2 and H Lyman-α brightnesses is more scattered (Figures 4a and 4b) compared to the relationship between the H_2 two bands (Figure 4c). Table 1 summarizes the correlation coefficients of these relationships for each auroral region separately. The correlation values are derived using linear values except for Figure 6a using logarithmic values.

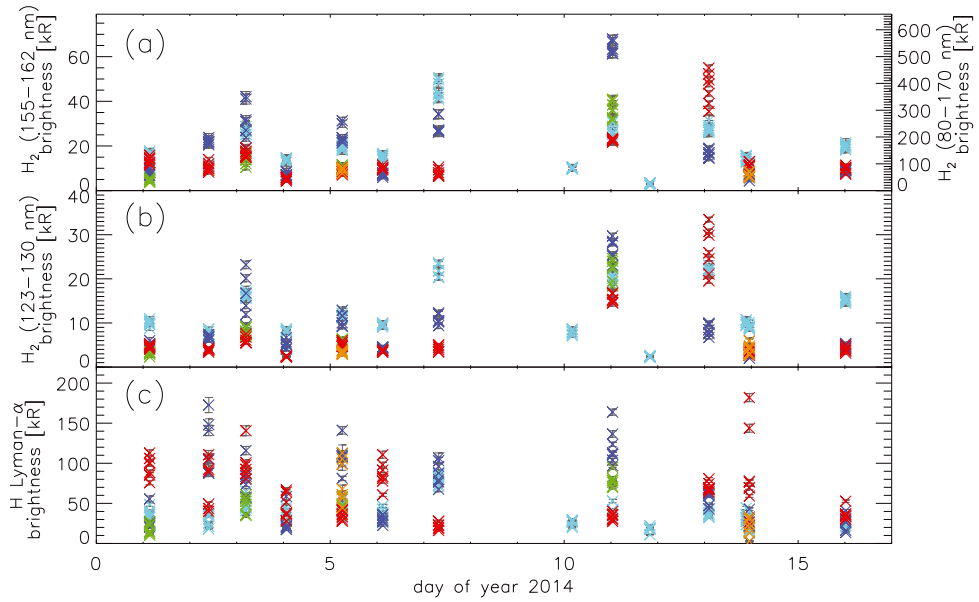

Figure 3: The time variations of the auroral brightness emitted at wavelengths of (a) 155–162 nm, (b) 123–130 nm, and (c) H Lyman-α corrected for hydrocarbon absorption averaged over each 30 s, with error bars (grey vertical lines). The point colors correspond to the auroral regions: the main aurora on the disk (blue), the main auroral emission at the limb (light blue), high latitude emission (red), low-latitude emission (green), and Io footprint/tail (orange). The estimated total brightness over 80–170 nm is shown on the right axis of Figure 3a.

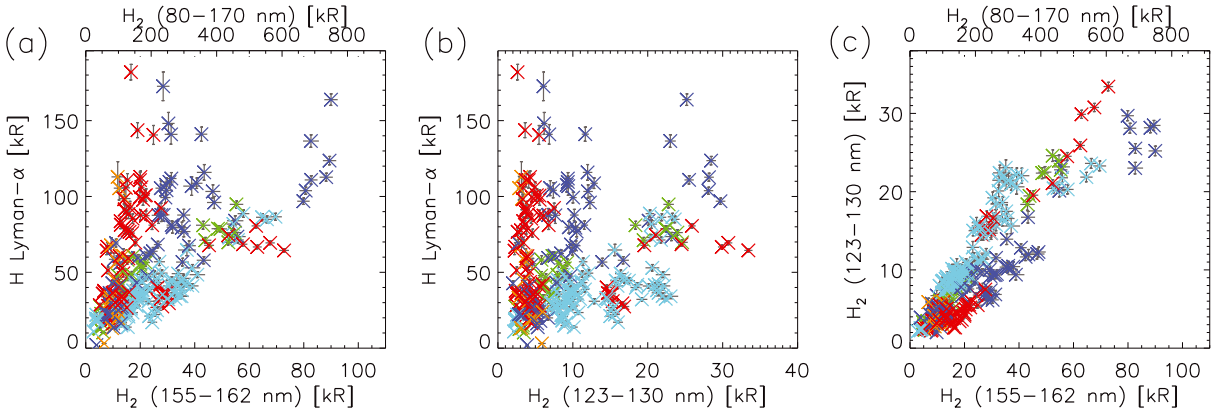

Figure 4: The brightness ratios of H Lyman-α to (a) H_2 emission over 155–162 nm and (b) H_2 emission over 123–130 nm, and (c) brightness of H_2 emission over 155–162 nm to H_2 emission over 123–130 nm. The point colors correspond to the auroral regions, as in Figure 3.

Table 1: Correlation coefficients of Figures 4a–4c, 5, and 6a

correlation coef.	Fig.4a	Fig.4b	Fig.4c	Fig.5a	Fig.5b	Fig.5c	Fig.5d	Fig.6a
main aurora at limb	0.87	0.62	0.90	-0.64	0.33	-0.81	0.33	-0.68
main aurora on disk	0.75	0.59	0.96	-0.67	0.053	-0.68	0.053	-0.39
low-lat. emission	0.90	0.87	0.99	-0.82	0.25	-0.92	0.25	0.14
high-lat. emission	0.20	-0.01	0.95	-0.61	-0.46	-0.75	-0.46	-0.78
Io footprint/tail	0.57	-0.62	-0.22	0.56	-0.66	0.57	-0.66	-0.99

The H/H_2 (80–170 nm) brightness ratio displayed in Figure 5a decreases with increasing H_2 brightness, from 0.8 for small H_2 brightness around 20 kR, to 0.1 for large H_2 brightness at $\sim$ 500 kR. The $H/\{H+H_2$ (120–123 nm)$\}$ brightness ratio also decreases as a function of the H_2 brightness, from 0.95 to 0.65 as shown in Figure 5c. This trend is commonly seen as a negative correlation coefficient for the main aurora and high- and low- latitude emissions (Table 1).

We also plot the correlation between the inversed brightness ratios and the FUV CR in Figures 5b and 5d. The reversed brightness ratio, H_2/H, represents higher energies by larger ratio values for both parameters. The points are significantly scattered and the correlation level between the two parameters is low (correlation coefficients of ¡0.33, Table 1). We note that for the main auroral emission at the limb shown with light blue dots, the FUV CR variation is small, between 1.3 and 3, while the $H_2(80-170$ nm$)/H$ brightness ratio increases from 1 to 8 in Figure 5b. At the limb, the CR usually becomes small due to the contribution of the emission above the HC layer. On the other hand, hydrogen atoms exist at higher altitude, so that the H_2/H ratio should vary with emission altitude.

The relationship between the auroral electron energy derived from the H/H_2 brightness ratio and electron flux is shown in Figure 6, with color–distinguishing auroral regions (Figure 6a) and HST observation orbits (Figure 6b). The electron flux clearly decreases

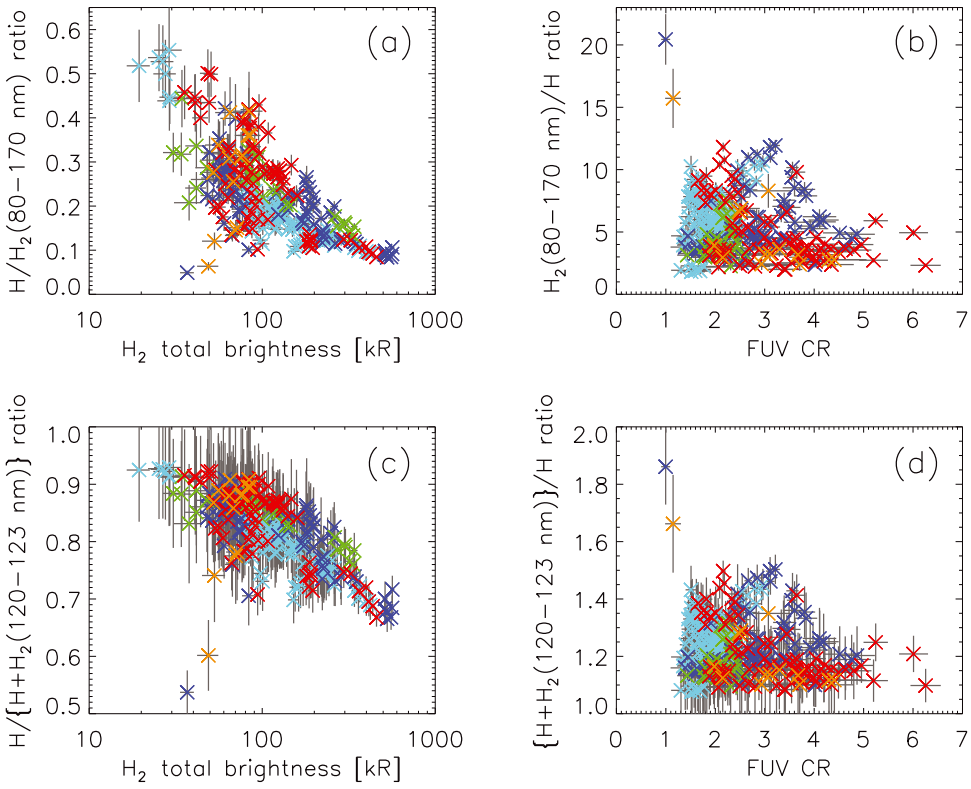

Figure 5: Brightness ratios of H Lyman-α to (a)(b) total H_2 emission over 80−170 nm and to (c)(d) total H and H_2 emission over 120−123 nm as a function of total H_2 emission over 80−170 nm and as a function of hydrocarbon color ratio, respectively, with error bars (gray lines). The point colors correspond to the auroral regions, as in Figure 3.

with increasing electron energy, from several μA/m^2 at a few 0.1s of keV to ∼0.3 μA/m^2 at several keV. In addition, for 1−3 μA/m^2 the energy coverage broadens over 0.6−10 keV. The main aurora and the high latitude emission spread over a wide parameter range, while the low- latitude emission (in green) is concentrated at the latter 1−3 μA/m^2 and

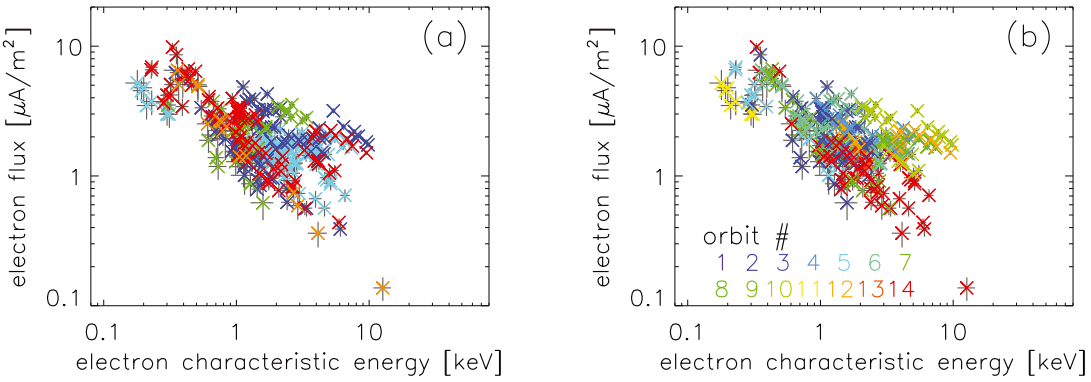

Figure 6: Relationship between the auroral electron characteristic energy and electron flux, with color distinguishing (a) auroral regions and (b) HST observation orbits, with error bars (gray lines). For Figure 6a, the point colors correspond to the auroral regions, as in Figure 3.

0.6−10 keV region (Figure 6a). The Io footprint and tail regions (in orange) in this analysis does not contain the broaden features and show decreasing electron flux with increasing electron energy (Figure 6a).

For the day–to–day variation (Figure 6b), the parameters observed during the first half of the interval (blue points) are concentrated at the low energies and high electron fluxes, while those observed during the last two days (red) are concentrated at high energies and low electron fluxes. The main aurora brightness decreases over the 14 days–long time interval [Badman et al., 2016]. The points at electron flux of 1−3 μA/m^2 and electron energy of 4−10 keV, which fall outside the general anti-correlated energy–flux relation, are contributed by the main aurora at the limb on orbits #7 (January 7, 2014), by the main aurora on the disk on #9 (January 11), and by the high-latitude emission on #11 (January 13). They are the brightest emissions crossed by the spectral slit (Figure 2). The observations on orbits #7 and #9 (orbit #11) are associated with the bright (medium) polar emission [Badman et al., 2016].

4 Discussion

4.1 Comparison with FUV CR

As shown in Figures 5b and 5d, a correlation between the inverse of H/H_2 and FUV CR is not obvious. The former is sensitive to low energy electrons (<a few keV), while the latter is sensitive to high energy electrons (>a few 10s keV), so that this results indicates that precipitation of low energy electrons is not simply correlated with that of high energy electrons.

4.2 Variation among auroral regions

As seen in Figure 5, the high latitude and main auroral emissions cover wide parameter ranges of the H_2 total brightness, i.e., energy flux, H/H_2 ratio, and FUV CR. In addition, many samples indicating the low-energy (< 1 keV) flux are also detected in the high-latitude region. This would reflect the non-uniform and temporal variations of the polar region. The low-latitude emission covers intermediate parameter ranges (Figures 5 and 6), which would reflect its dynamic variation with magnetospheric activities [e.g. Kimura et al., 2017].

4.3 Comparison with Saturn

The decreasing trend (as a function of the brightness of H_2) and the ratio values are qualitatively similar to those found for Saturn, although H_2 brightness values at Jupiter are much larger than at Saturn. For the Saturn case, the electron energy and flux relationship show two different behaviors below and above ∼5 keV. Below 5 keV, the electron flux decreases with increasing energy, while above 5 keV electron, the electron flux increases with electron energy [Tao et al., 2014]. In the case of Jupiter, the decreasing

trend continues until electron energies of ∼10 keV, while the 1−3 μA/m^2 and 4−10 keV region might mark a transition with the increasing trend. Estimated electron energies extend up to ∼10 keV for this analysis of Jupiter, while they reach ∼30 keV for Saturn. This reduced energy coverage may make it difficult to identify any increasing trend with higher energies for the Jupiter analysis shown here. In addition, the thermal component of the magnetospheric source plasma is ∼2.5 keV for Jupiter [Scudder et al., 1981], which is larger than the 0.01−1 keV at Saturn [Arridge et al., 2009]. Since the start of the increase corresponds to the source temperature, this higher energy of the source plasma could shift the increasing trend towards higher energy.

5 Summary and conclusions

We have investigated the relationship between the H/H$_2$ brightness ratio and total H$_2$ brightness of Jupiter aurora observed by HST/STIS. The brightness ratio decreases with the H$_2$ total brightness, like in the case of Saturn. The precipitating flux of auroral electrons mainly decreases with increasing energy, as also observed for Saturn. Our analysis also suggests the possibility that statistical analyses of the H/H$_2$ brightness ratio can provide new information on Jovian auroral electron energy in their low energy range 0.1−10 keV. Recently, Jupiter's polar orbiter Juno started to observe in-situ auroral electrons. Comparison with these unique observations will enable us to check and validate the above described method in a near future.

Acknowledgments. This work is based on observation made with the NASA/ESA Hubble Space Telescope (observation ID: GO13035), obtained at the Space Telescope Science Institute, which is operated by AURA, Inc. for NASA. This work was supported by JSPS KAKENHI grant JP15K17769. LL, RP, and NA are supported by CNES. SVB was supported by STFC Fellowship ST/M005534/1. We thank the referees for their productive and valuable comments. The Editors also thank the two anonymous referees for their help in evaluating this paper.

References

Arridge, C. S., et al. (14 co–authors), Plasma electrons in Saturn's magnetotail: Structure, distribution and energization, *Planet. Space Sci.*, **509**, 2032–2047, 2009.

Badman, S. V., et al. (16 co–authors), Weakening of Jupiter's main auroral emission during January 2014, *Geophys. Res. Lett.*, **43**, 988–997, 2016.

Bonfond, B., J. Gustin, J.–C. Gérard, D. Grodent, A. Radioti, B. Palmaerts, S. V. Badman, K. K. Khurana, and C. Tao, The far-ultraviolet main auroral emission at Jupiter–Part 2: Emission profile, *Ann. Geophys.*, **33**, 1211–1218, doi:10.5194/angeo-3312112015, 2015.

Gérard, J.–C., J. Gustin, D. Grodent, J. T. Clarke, and A. Grard, Spectral observations of transient features in the FUV Jovian polar aurora, *J. Geophys. Res.*, **108**, A8, id.1319, doi:10.1029/2003JA009901, 2003.

Gérard, J.–C., B. Bonfond, D. Grodent, A. Radioti, J. T. Clarke, G. R. Gladstone, J. H. Waite, D. Bisikalo, and V. I. Shematovich, Mapping the electron energy in Jupiter's aurora: Hubble spectral observations, *J. Geophys. Res.*, **119**, 9072–9088, 2014.

Gladstone, G. R., M. Allen, and Y. L. Yung, Hydrocarbon photochemistry in the upper atmosphere of Jupiter, *Icarus*, **119**, 1–52, 1996.

Grodent, D., J. H. Waite Jr., and J.–C. Gérard, A self-consistent model of the Jovian auroral thermal structure, *J. Geophys. Res.*, **106**, A7, 12933–12952, 2001.

Gustin, J., J.–C. Gérard, W. Pryor, P. D. Feldman, D. Grodent, and G. Holsclaw, Characteristics of Saturn's polar atmosphere and auroral electrons derived from HST/STIS, FUSE and Cassini/UVIS spectra, *Icarus*, **200**, 176–187, 2009.

Gustin, J., D. Grodent, L. C. Ray, B. Bonfond, E. J. Bunce, J. D. Nichols, and N. Ozak, Characteristics of north Jovian aurora from STIS FUV spectral images, *Icarus*, **268**, 215–241, 2016.

Gustin, J., D. Grodent, A. Radioti, W. Pryor, L. Lamy, and J. Ajello, Statistical study of Saturn's auroral electron properties with Cassini/UVIS FUV spectral images, *Icarus*, **284**, 264–283, 2017.

Kimura, T., et al. (13 co–authors), Transient brightening of Jupiter's aurora observed by the Hisaki satellite and Hubble Space Telescope during approach phase of the Juno spacecraft, *Geophys. Res. Lett.*, **44**, 4523–4531, doi:10.1002/2017GL072912, 2017.

Lamy, L., R. Prangé, W. Pryor, J. Gustin, S. V. Badman, H. Melin, T. Stallard, D. G. Mitchell, and P. C. Brandt, Multispectral simultaneous diagnosis of Saturn's aurorae throughout a planetary rotation, *J. Geophys. Res.*, **118**, 4817–4843, 2013.

Lystrup, M. B., S. Miller, N. Dello Russo, R. J. Vervack Jr., and T. Stallard, First vertical ion density profile in Jupiter's auroral atmosphere: Direct observations using the Keck II telescope, *Astrophys. J.*, **677**, 790–797, 2008.

Melin, H., and T. S. Stallard, Jupiter's hydrogen bulge: A Cassini perspective, *Icarus*, **278**, 238–247, 2016.

Menager, H., M. Barthélemy, and J. Lilensten, H Lyman α line in Jovian aurora: Electron transport and radiative transfer coupled modeling, *Astron. Astrophys.*, **509**, id.A56, 9 pp., 2010.

Perry, J. J., Y. H. Kim, J. L. Fox, and H. S. Porter, Chemistry of the Jovian auroral ionosphere, *J. Geophys. Res.*, **104**, 16541–16565, doi:10.1029/1999JE900022, 1999.

Rego, D., R. Prangé, and L. Ben Jaffel, Auroral Lyman α and H_2 bands from the giant planets: 3. Lyman α spectral profile including charge exchange and radiative transfer effects and H_2 color ratios, *J. Geophys. Res.*, **104**, E3, 5939–5954, doi:10.1029/1998JE900048, 1999.

Scudder, J. D., E. C. Sittler Jr., and H. S. Bridge, A survey of the plasma electron environment of Jupiter: A view from Voyager, *J. Geophys. Res.*, **86**, 8157–8179, 1981.

Tao, C., L. Lamy, and R. Prangé, The brightness ratio of H Lyman-α/H_2 bands in FUV auroral emissions: A diagnosis for the energy of precipitating electrons and associated magnetospheric acceleration processes applied to Saturn, *Geophys. Res. Lett.*, **41**, 6644–6651, 2014.

Tao, C., T. Kimura, S. V. Badman, G. Murakami, K. Yoshioka, F. Tsuchiya, N. André, I. Yoshikawa, A. Yamazaki, D. Shiota, H. Tadokoro, and M. Fujimoto, Variation of Jupiter's aurora observed by Hisaki/EXCEED: 1. Observed characteristics of the auroral electron energies compared with observations performed using HST/STIS, *J. Geophys. Res.*, **121**, 4041–4054, doi:10.1002/2015JA021271, 2016a.

Tao, C., T. Kimura, S. V. Badman, N. André, F. Tsuchiya, G. Murakami, K. Yoshioka, I. Yoshikawa, A. Yamazaki, and M. Fujimoto, Variation of Jupiter's Aurora observed by Hisaki/EXCEED: 2. Estimations of auroral parameters and magnetospheric dynamics, *J. Geophys. Res.*, **121**, 4055–4071, doi:10.1002/2015JA021272, 2016b.

Uno, T., Y. Kasaba, C. Tao, T. Sakanoi, M. Kagitani, S. Fujisawa, H. Kita, and S. V. Badman, Vertical emissivity profiles of Jupiter's northern H_3^+ and H_2 infrared auroras observed by Subaru/IRCS, *J. Geophys. Res.*, **119**, 10219–10241, 2014.